Anti-Corrosion Coatings on SS 304 by Incorporation of Pr_6O_{11}-TiO_2 in Siloxane Network

K. Jeeva Jothi, K. Palanivelu*

Central Institute of Plastics Engineering and Technology (CIPET), Guindy, Chennai 600032, Tamil Nadu, India
** e-mail: kpalanivelucipet@gmail.com*

This paper describes an attempt to develop anticorrosive siloxane coatings based on Pr_6O_{11}-TiO_2 composite films for SS 304 substrate by sol-gel technique. We demonstrate for the use of praseodymium oxide doped Titanium oxide (Pr_6O_{11}-TiO_2) nanocomposites loaded in a hybrid sol-gel layer, to effectively protect the underlying steel substrate from corrosion attack. The influence of Pr_6O_{11}-TiO_2 gives the surprising aspects based on active anti-corrosion coatings. The silica sol was treated with Pr_6O_{11}-TiO_2 to achieve different level of add-on i.e.) 0–1 wt% of nanocomposites. The influence of different weight percent of nanocomposites on silica matrix for anticorrosion performance was investigated by Electrochemical Impedance Spectroscopy (EIS). Pr_6O_{11}-TiO_2 nanocomposites loaded in a hybrid sol-gel layer effectively protect the underlying substrate from corrosion attack. The results showed significant improvement in anticorrosion property for higher add-ons up to the optimized percent of nanocomposites. Furthermore, Transmission Electron Microscopy (TEM) and Scanning Electron Microscope Microscopy (SEM) were used to characterize the surface morphology of doped and undoped coatings. The studied showed a synergistic effect between Pr_6O_{11}-TiO_2 and siloxane matrix has leads to a self-healing coatings.

Keywords: sol-gel process, anticorrosion, nanocomposites, EIS.

УДК 621.373.826

Graphical abstract

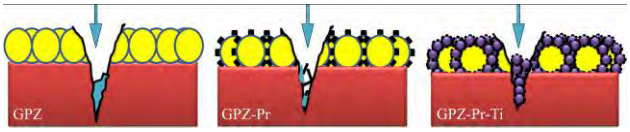

INTRODUCTION

In recent years considerable work has been done on organic-inorganic hybrid materials for enhanced coating properties like thermal stability, corrosion resistance and scratch and abrasion resistance. The sol-gel route is the most commonly employed methods for the preparation of such hybrid coatings at macro/micro-scale. In the sol-gel process, for synthesis of inorganic part various organo metal precursors based on silicone, titanium, aluminium, and zirconium have been widely used [1]. Titanium oxide is a functional ceramic material that has attracted much attention in the last a few decades due to its unique properties [2–4]. In most cases, the material is used in the form of thin films or coatings on various substrates to study anticorrosive and light conduction properties [5]. In order to overcome the limitation of single component oxide layer on coatings, incorporation of nanocomposites may improve the surface protection [6].

Many attempts have been made to modify TiO_2 coatings by doping it with metallic and nonmetallic ions. A well-known corrosion inhibitor, CeO_2 is a promising choice to be incorporated into oxide films for a composite coating [7]. Synthetic ceramic coatings based on TiO_2 have been used to modify the surface of austenitic stainless steels and other biomedical metals. Titania coatings are demonstrated to be hard, corrosion resistant and biocompatible material with photo-induced hydrophilicity [8–10]. TiO_2 has excellent chemical stability, heat resistance and low electron conductivity, making it an excellent anti-corrosion material. But the pure TiO_2 films are mostly used in catalyst chemistry while very few have been reported for protective coatings on steel substrate [11]. Organic-inorganic multilayer coating containing organically modified silicates, epoxy resins and TiO_2 nanocontainers loaded with 8-hydroxyquinoline was produced on AA2024-T3 substrates for anti-corrosion behavior [12].

One of the most important advantages of the sol-gel method is the possibility of using simple coating operations like immersion of the object in the solution followed by drying. The sol-gel deposition procedure requires relatively lower temperature when compared to chemical vapor deposition and therefore it is considerably less expensive. Perhaps the most important advantage of the sol-gel method is the possibility to control microstructure of the films [13].

In recent year's praseodymium compounds have attracted great attention as luminescent materials, catalysts, high-k gate dielectric materials, and opti-

cal filters [14]. This work reports the performance of active anti-corrosion coatings by forming a core-shell of SiO_2 @ Pr_6O_{11}-TiO_2 hybrid materials. The light rare earth elements Cerium, Praseodymium, and Neodymium have similar properties. The main reason for the choice praseodymium oxide is that it develops a green oxide coating when exposed air and thus may show corrosion resistance. The Pr_6O_{11} modified with TiO_2 could find a wider application in the area of paints and coatings. The anti-corrosion behavior of SiO_2 @ Pr_6O_{11}-TiO_2 hybrid coating on steel substrates was investigated in 0.5M of NaCl solution by electrochemical measurements. The results were utilized to quantify the corrosion protection efficiency and estimate the extent of coating degradation. To the best of our knowledge SiO_2 @ Pr_6O_{11}-TiO_2 hybrid materials have not been reported earlier. The synergistic effect of SiO_2 @ Pr_6O_{11}-TiO_2 renders a better anticorrosion behavior on the surface of coated substrate.

MATERIALS AND METHODS

Materials

The chemicals used for the preparation of silica sols using the precursors, such as 3–glycidoxypropyltrimethoxysilane (GPTMS), octyltriethoxysilane (OTES), N-[3-(trimethoxysilyl) propyl]aniline (TMPA) and zirconium (IV) propoxide (TPOZ) from Aldrich®, 2–butoxy ethanol ($C_6H_{14}O_2$), Titanium isopropoxide (Ti(OCH $(CH_3)_2)_4$), isopropanol (C_3H_7OH) and hydrochloric acid (HCl), from MERCK, praseodymium oxide (Pr_6O_{11}) from s. d. Fine CHEM. LIMITED, Mumbai and double distilled water were used throughout the experiments.

Substrate preparation

Stainless steel 304 (SS) with composition of Fe-Cr-Ni is 70–20–10 wt% had cut into 4 cm × 2 cm pieces. The SS substrates were polished with increasing grades of silicon carbide emery papers from 140 to 1200, were sonicated in acetone for 20 min, and were dried in oven.

Preparation of Pr_6O_{11}-TiO_2

About 12.5 ml of Titanium isopropoxide and 80 ml of isopropanol were taken to form a homogeneous solution. To the latter solution, 0.243g of Pr_6O_{11} (9 wt%) was dispersed to get a dark brown color solution. The above solution was stirred for 5h, while stirring 1.5 mL of water (for hydrolysis) has been added in drop wise and ensures the complete precipitation. Then the mixture was transferred into a teflon lined stainless steel autoclave, sealed and heated at 120°C for 12h at the pressure of 18 psi. Precipitated titanium hydroxide along with praseodymium hydroxide was filtered, washed with distilled water and ethanol, and dried in air oven at 90°C for 12h. The precipitate was sintered at 450°C for 4h in a muffle furnace to get Pr_6O_{11}-TiO_2.

Preparation of sol

The sol was prepared in two parts. In the first part a mixture of GPTMS/TMPA/OTES/2-butoxy ethanol in the molar ratio of 1:0.5:0.5:6 were taken and allowed to stir for 30 min at room temperature. The second part, TPOZ/2-butoxy ethanol/H_2O mixture was taken in the molar ratio of 0.5:6:4 and HCl (0.1M) was used as a catalyst and stirred separately for 30 min in ice bath to control the exothermic reaction. The part I was added drop wise into part II with constant stirring (To avoid agglomeration it must be added in drop wise). The whole set was in ice bath to avoid exothermic reaction.

The final sol was then stirred for 24h at room temperature. The resultant sol was a clear and homogeneous solution and referred as GPZ. GPZ was divided into two parts. To the different portion of the first part 0.25, 0.50, 0.75, and 1% by weight of Pr_6O_{11} was added. Then to the second part different concentration of Pr_6O_{11}-TiO_2 (0.25, 0.50, 0.75, and 1 wt%) was added. The above 8 compositions were stirred for 30 min and coated on the cleaned SS substrates by dip coating employing a withdrawal speed of 7 mm/s. The withdrawal speed above 7 mm/s, the coating gets peeled off while drying because of more thickness. So with the optimized withdrawal speed, films were dried at 150°C for 1h. The coated substrate (SS 304) was tested for corrosion and the composition was optimized. The sol with 0.75 wt% of Pr_6O_{11} and 0.5 wt% of Pr_6O_{11}-TiO_2 shows best results. These two samples were characterized further and referred as GPZ-Pr and GPZ-Pr-Ti are shown schematically in Figure 1.

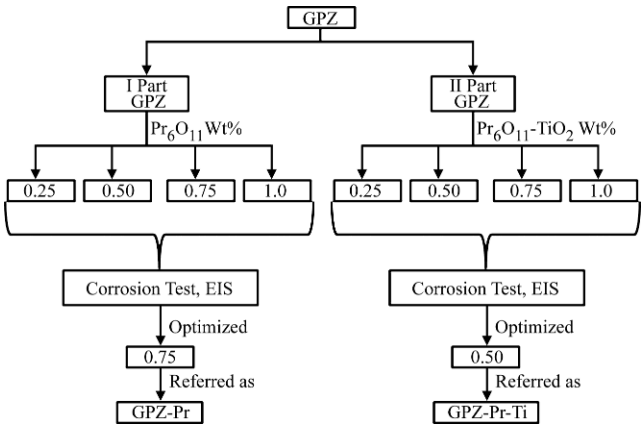

Fig. 1. Preparation of GPZ-Pr and GPZ-Pr-Ti.

Characterization Methods

The morphology, size and structure of the synthesized particles were characterized by Transmis-

sion Electron Microscopy (TEM) (JEOL TEM 2010 UHR model) and Scanning Electron Microscope Microscopy (SEM, ZEISS, EVO MA15) were employed to analyze the distribution of nanocomposites in the silica network. The crystallographic patterns of coated films were analyzed by X-Ray Diffractometer (XRD) (Shimadzu, XD–D1 diffractometer). Fourier Transform Infrared Spectroscopy (FTIR) (Avatar 303) which gave the information about various chemical bonds such as O-H, Si-C, C-H and Si-O-Si of the coated films. X-ray Photoelectron Spectra (XPS) of the catalysts were recorded using an ESCA-3 Mark II spectrometer (VG Scientific Ltd, England) using Al Kα (1486.6 eV) radiation as the source. Thickness of the films was characterized by Mitutoyo absolute digimatic. Polarization tests were carried out for SS 304 substrates in 0.5M of NaCl solution. The potentiodynamic measurements were taken within the range of potential –0.5 to +2.5 mV. The salt spray technique was carried out using 3.5 wt% of NaCl solution at 35°C, in a Salt Spray Chamber supplied by ATLAS.

RESULTS AND DISCUSSION

FTIR analysis

FTIR spectra of GPZ, GPZ-Pr and GPZ-Pr-Ti are shown in Figure 2. From the figure it is clear that after modifying the surface with the nanocomposites adsorption band corresponding to O-H (around 3425 cm^{-1}) increases gradually because of the hydrophilic nature of TiO_2. The characteristic bands at 1090 and 750 correspond to the stretching, and bending of Si-O bonds respectively. The adsorption peaks at 2927 cm^{-1} and 2863 cm^{-1} are associated with C-H stretching modes which indicate the presence of long alkyl groups in the silica network. The bands at 2926 cm^{-1} and 2861 cm^{-1} show the C-H asymmetric and symmetric stretching frequencies, and that at 1462 cm^{-1} and 694 cm^{-1} correspond to C-H symmetric and asymmetric bending, respectively. The O-H band in GPZ-Pr-Ti got increased compared to GPZ and GPZ-Pr, which confirms the hydrophilic nature of TiO_2. Because of the hydrophilic surface it's used for self-cleaning behavior. Peaks at 2926 and 2865 cm^{-1} correspond to C-H stretching mode also got increased compared to other peaks which confirms the good cross-linking between the nanocomposites and the silica network. The strong band observed at 1107 cm^{-1} indicates the presence of Si-O-Si moiety. The wave number of 940–960 and 1080–1105 cm^{-1} in Fig. 1 indicate the band for Ti-O-Si and Si-O-Si bond, respectively. The band for Ti-O-Si vibration is observed due to the higher quantity of SiO_2. The band intensity for Si-O-Si vibration increases with an increase of the silica content. This result suggests that the silica exists as a segregated amorphous phase in the anatase titania particles and some fraction of metal-O-metal bonding are Ti-O-Si. The broad absorption peak appearing near 3400 cm^{-1} relates to a stretching vibration of Ti-OH and Pr-OH group. Bands at 778 and 1276 cm^{-1} correspond to Si-CH_3 groups where the peaks got increased from GPZ to GPZ-Pr-Ti due to increase in cross-linking.

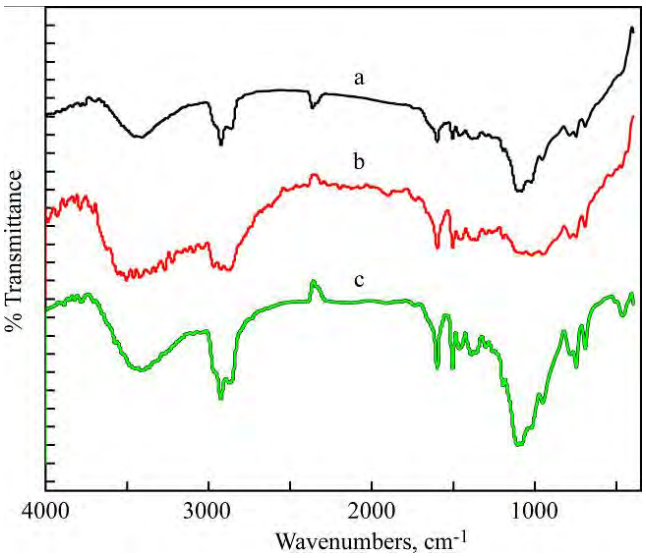

Fig. 2. FTIR spectra of (a) GPZ; (b) GPZ-Pr and (c) GPZ-Pr-Ti.

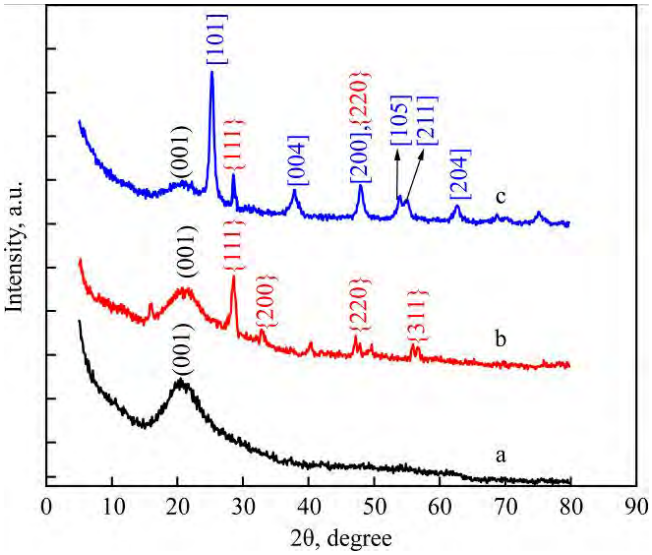

Fig. 3. XRD patterns of (a) GPZ; (b) GPZ-Pr and (c) GPZ-Pr-Ti.

XRD analysis

The phase structures of different siloxane coatings were investigated by X-Ray Diffractogram (XRD) as shown in Figure 3. The SiO_2 @ Pr_6O_{11}-TiO_2 core-shell nanostructured present in GPZ-Pr-Ti are compared with GPZ and GPZ-Pr. In GPZ no diffraction regards nanocomposites, only one broad peak around 20° corresponds to the typical diffraction of amorphous SiO_2 group [001]. In Fig. 3b except the broad peak around 20°, all the

other peaks can be attributed to the pure cubic phase of Pr_6O_{11}. The 2θ peaks at the values of 28.05, 32.62, 46.74 and 55.74° correspond to the diffraction planes of [111], [200], [220] and [311] of the crystalline Pr_6O_{11} species respectively. The diffraction peaks in Fig. 3c show the mixed patterns of TiO_2 and Pr_6O_{11}. For TiO_2 at 25.22, 37.74, 47.93, 53.85, 55.13 and 62.73° corresponds to the diffraction planes of [101], [004], [200], [105], [211] and [204] of anatase TiO_2, respectively. [(JCPDS Card No. 71–1169]. Few peaks of Pr_6O_{11} absolutely match with Pr_6O_{11}-TiO_2@SiO_2, but no intense peak of Pr_6O_{11} is shown in GPZ-Pr-Ti, this is probably due to the low Pr_6O_{11} doping content and the data may also imply that the Pr_6O_{11}-TiO_2 oxides are well dispersed within the SiO_2 phase. There is no remarkable shift in the diffraction peaks, and the other crystalline impurities are not observed. After the addition of nanocomposites there is an increase in crystalline behavior of materials. It is important that the increase in crystalline is the most exaggerated when the concentration of nanocomposites increases beyond the optimized ratio and it may cause defects to the coating. Beside the crystallinity, stress and strain are other important parameters in coating characterization.

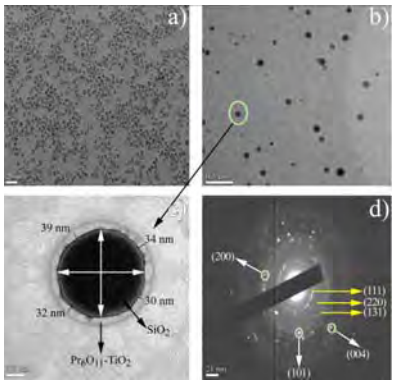

Fig. 4. TEM images of (a) Pr_6O_{11}-TiO_2; (b) GPZ-Pr-Ti-0.2 μm; (c) GPZ-Pr-Ti-100 nm and (d) SAED pattern.

TEM

To visualize the core-shell structure of SiO_2 @ Pr_6O_{11}-TiO_2 particles TEM was performed. Representative TEM micrographs of the SiO_2 particles coated by Pr_6O_{11}-TiO_2 shells are shown in Figure 4. The structural morphology of pure Pr_6O_{11}-TiO_2 nanocomposites in the absence of siloxane network has shown in Figure 4a. The core-shell structure of the SiO_2 @ Pr_6O_{11}-TiO_2 particles can be seen clearly due to the different electron penetrability for the cores and shells (Fig. 4b,c). The cores are black spheres with an average thickness of 450 nm (SiO_2) and the shells have gray color with an average thickness of 45 nm (Pr_6O_{11}-TiO_2). The electron diffraction rings with some disorder in Fig. 3d are shown, just to demonstrate the coexistence of crystalline phase (Pr_6O_{11}-TiO_2) and amorphous phase (SiO_2) in the interface region of the core-shell particles. Selected area electron diffraction pattern (SAED) from the SiO_2 matrix along with Pr_6O_{11}-TiO_2 is also included in Figure 4d. The three rings that are clearly visible in the diffraction pattern correspond to the first three strongest reflections of Si that were formed by reflections from the {111}, {220} and {311} atomic planes with a spacing of 0.314, 0.192 and 1.64 nm respectively. The SAED pattern exhibits a number of bright spots arranged in concentric rings, which correspond to the {111}, {220} and {311} planes of SiO_2.

SEM

The surface morphology of the prepared sol-gel composites was examined using FE-SEM analysis was presented in Figure 5. The morphology of GPZ shows the large particles of siloxane and GPZ-Pr shows the large particles of siloxane with layered flake structure due to Pr_6O_{11} was shown in Fig. 5a,b, which are more loosely packed. It looks like a unique body shape of a Sperm Whale (given in inset Figure 5a). But in Fig. 5c,d, SiO_2 @ Pr_6O_{11}-TiO_2 shows the more densely packed with the uniform distribution of nanocomposites throughout the siloxane network. The surface morphology of GPZ-Pr-Ti indicates the advantageous effect of SiO_2 functionalization on surface structure. There is an increased tendency for the presence of numerous primary particles of small diameter in Pr_6O_{11}-TiO_2 around SiO_2. It is interesting to note that modification with silicone practically restricted the tendency for particle agglomeration. Energy dispersive spectroscopy is generally accurate up to trace amounts of metal present in the surface of base materials. The EDS recorded from the selected area (Fig. 5e) reveals the presence of Si, Ti, Zr and O in the catalyst. Zirconium appears due to the presence of zirconium (IV) propoxide precursor present in the sol (Figure 5e).

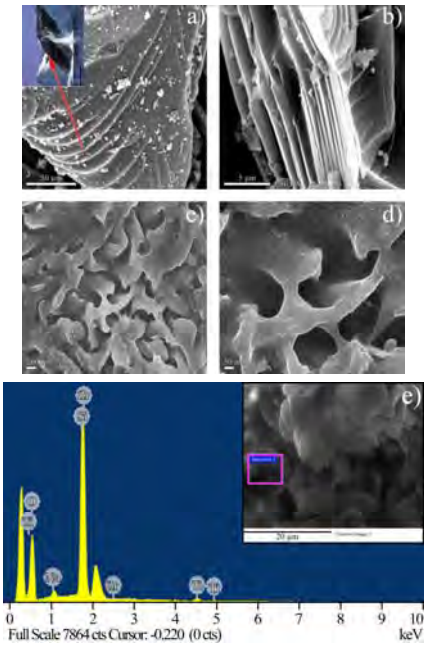

Fig. 5. SEM images of (a) GPZ; (b) GPZ-Pr; (c) GPZ-Pr-Ti (50 KX); (d) GPZ-Pr-Ti (100 KX) and (e) EDAX for GPZ-Pr-Ti.

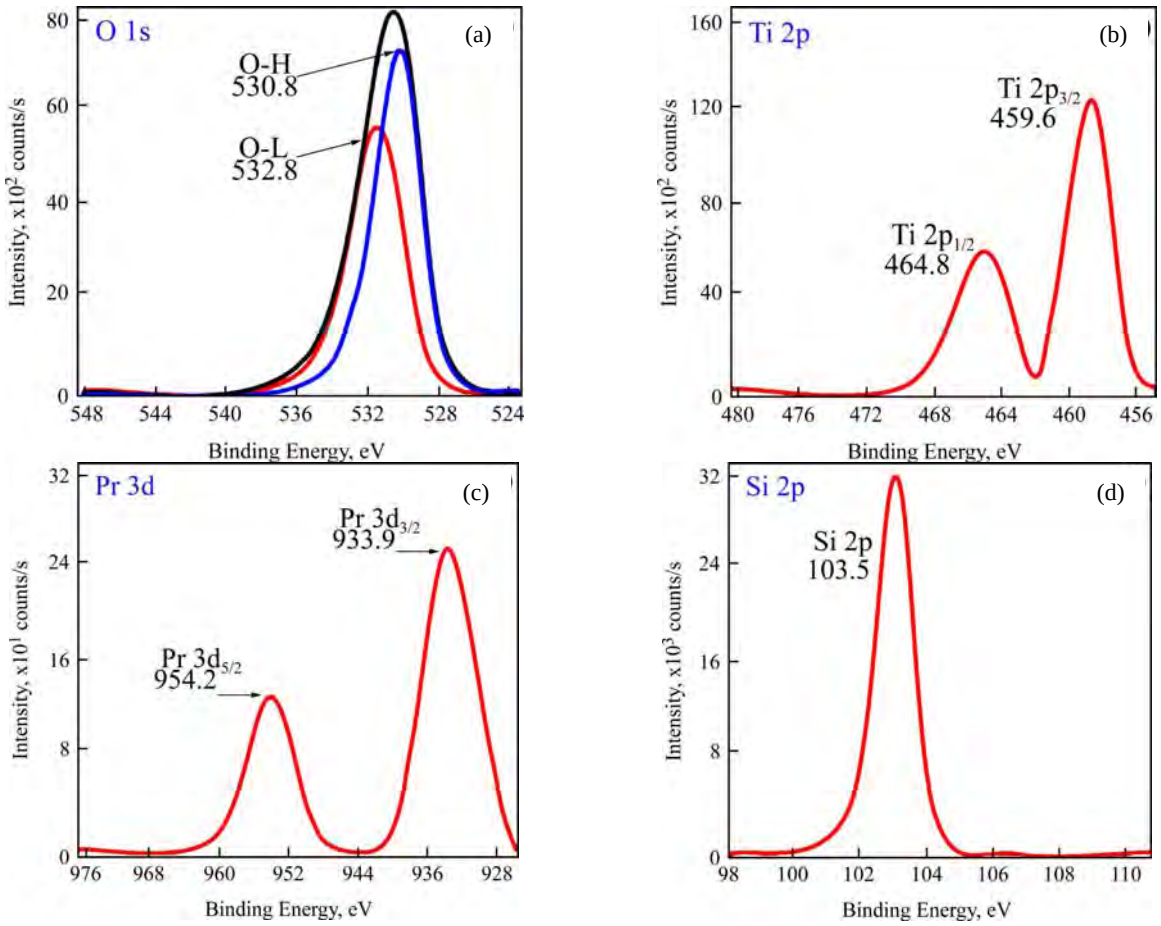

Fig. 6. XPS analysis of SiO_2 @ Pr_6O_{11}-TiO_2 matrix (a) survey spectrum; (b) O 1s; (c) Ti 2p; (d) Pr 3d and (e) Si 2p.

XPS analysis

XPS is a sensitive tool for the analysis of the chemical compositions of materials and hence XPS spectra of the SiO_2 @ Pr_6O_{11}-TiO_2 composites were recorded in order to gain more structural information as shown in Figure 6. The O 1s profile is asymmetric and can be fitted to two symmetrical peaks α and β located at 530.8 and 532.8 eV, respectively, indicating two different kinds of O species in the sample (Figure 6a). The peaks α and β should be associated with the lattice oxygen (O_L) of TiO_2 and chemisorbed oxygen (O_H) caused by the surface hydroxyl [15] respectively. In Fig. 6b,c,d, the high-resolution binding energy spectra for Ti, Pr and Si species are shown, respectively. Two symmetric peaks at 459.6 and 464.8 eV in the high resolution XPS spectrum of Ti 2p are assigned to Ti $2p_{3/2}$ and Ti $2p_{1/2}$, indicating the existence of Ti^{2+} in the Pr_6O_{11}-TiO_2 (Fig. 6b) [16]. Two symmetric peaks at 933.9 and 954.2 eV, which represent the $3d_{3/2}$ and $3d_{5/2}$ electrons of Pr, (Fig. 6c) respectively. According to the results of He et al., we assign the signals at ca. 933.9 and 954.2 eV to Pr^{4+} [17]. There is an increase in the values of the binding energy of Ti 2p and Pr 3d but a slight decrease in the value of the binding energy of Si 2p. So interaction should exist among TiO_2, Pr_6O_{11} and SiO_2 which cause the change of binding energies of Ti, Pr and Si, i.e., it may confirm that SiO_2 @ Pr_6O_{11}-TiO_2 thereby leading the interaction to a certain extent among them.

Thickness measurements

Thickness of the silane/nanoparticles films was estimated using Mitutoyo absolute digimatic. Nanoparticles has played an important role to increase the viscosity of the sol (thickness is directly propositional to viscosity). The thickness of GPZ-Pr films is higher than GPZ films (GPZ – 2.02 μm and GPZ-Pr – 2.76 μm). Moreover the formation of core-shell (Pr_6O_{11}-TiO_2) further increased the film thickness to 3.55 μm. These may be attributed to increase in viscosity of the solution in presence of nanoparticles, thus giving a thick coating at the same withdrawal speed. Since no agglomeration of particles was observed in the silane coating and it may be concluded that, the coating is homogenous with uniform thick films and make the way easier to prevent it corroding.

Corrosion studies

EIS measurements were carried out to evaluate the coating performance and corrosion resistance of uncoated and coated SS 304 in 0.5M of NaCl solution. Nyquist plot for bare SS 304, GPZ, GPZ-Pr

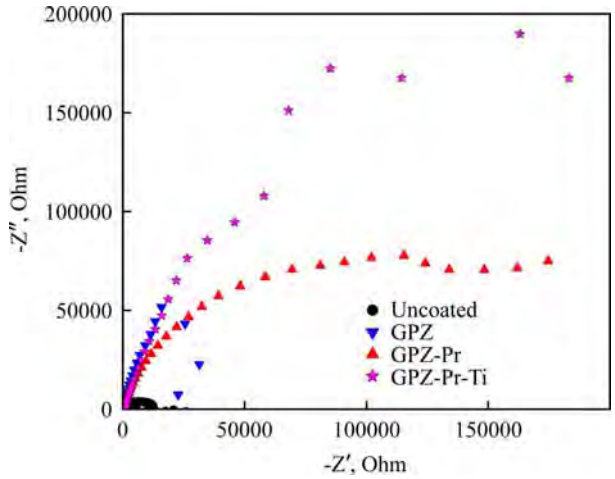

Fig. 7. Nyquist plots for Uncoated, GPZ, GPZ-Pr and GPZ-Pr-Ti.

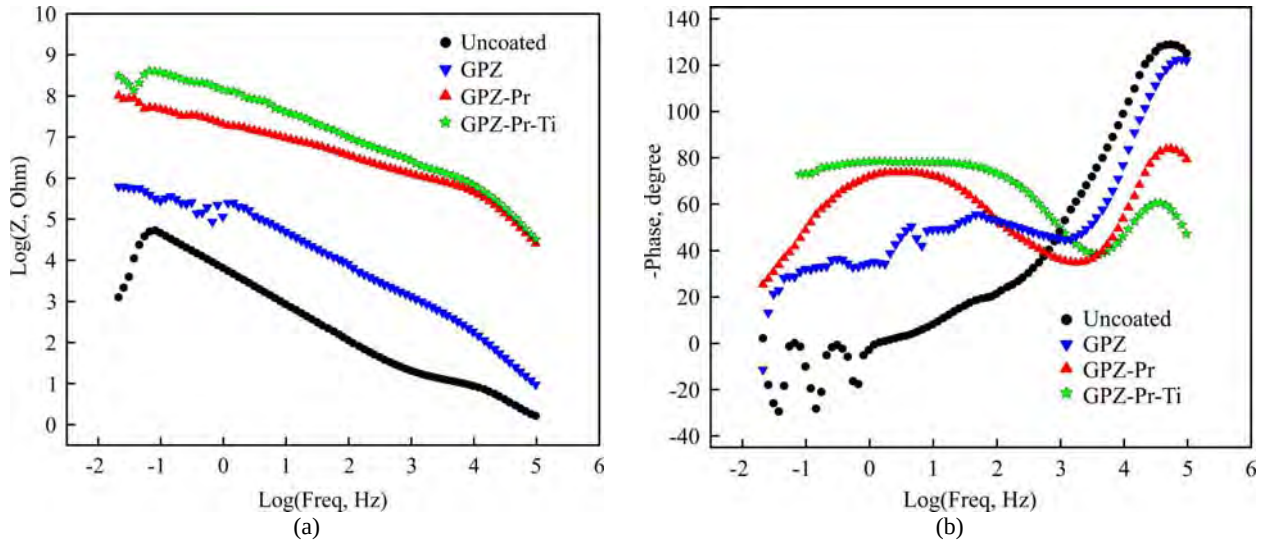

Fig. 8. Bode plots showing the (a) absolute impedance and (b) phase angle.

and GPZ-Pr-Ti are shown in Figure 7. The bare SS 304 showed a depressed semicircle which represents the surface heterogeneity and interfacial (corrosion) process of the system, i.e., charge transfer resistance due to metal corrosion and the double layer capacitance of the liquid/metal interface [18]. Therefore, all coating systems have higher corrosion resistance than the control (bare SS 304) which demonstrates poor barrier properties resulting in insufficient corrosion resistance. The highest resistance value was obtained for the GPZ-Pr-Ti coating, followed by the lowest resistance values of uncoated and GPZ. The incorporation of nanocomposites allows homogeneous dispersion within the sol-gel matrix resulting in a better integrity and stability of the coating matrix. Furthermore, nanoparticles Pr_6O_{11} (GPZ-Pr) provide larger interfacial area between the sol-gel matrix and the nanoparticles surface that allows the diffusion of aggressive electrolyte species towards the metal substrate. To make the diffusion path small the Pr_6O_{11} were doped with TiO_2 and make the core-shell around the SiO_2 particle then there will be a less interfacial area between the sol-gel matrix and the nanoparticles surface. Consequently, less diffusion paths are present in the coatings GPZ-Pr-Ti which restrict the diffusion of aggressive electrolyte species towards the metal substrate. The good barrier properties of the coatings with the nanocomposites (GPZ-Pr-Ti) give the good inhibiting effect. The positive effect of the inhibiting species relies on their release upon the onset of corrosion. The release inhibitor molecules form a layer on the metal surface, which terminate the corrosion processes and restore partially the coating barrier properties in the damaged coating area.

The impedance spectra of SS 304 coated with intact sol-gel coatings containing nanocomposites in 0.5M of NaCl solution are represented in the form of Bode plots in Figure 8. It could be visualized, GPZ-Pr-Ti showed increases in maximal phase angle value for better coating and barrier properties (Figure 8b). The high frequency time constant can be ascribed to the sol-gel coating capacitance and the low frequency time constant to the capacitance of the intermediate oxide layer at the metal-coating interface. As a result, sufficient coating barrier properties are revealed by good pore resistance resulting in higher $|Z|$ values measured for the

GPZ-Pr-Ti coatings, which account for the better barrier properties than the other coatings (Figure 8a).

The potentiodynamic polarization curves for Bare SS 304, GPZ, GPZ-Pr and GPZ-Pr-Ti in 0.5M of NaCl solution are shown in Figure 9. These polarization curves showed the positive shift in the corrosion potential (E_{corr}) and substantial reduction in corrosion current (I_{corr}) up to Pr_6O_{11}-TiO_2 @ SiO_2. The values of E_{corr} increase from Bare SS 304 to GPZ-Pr-Ti. If the concentrations of Pr_6O_{11}-TiO_2 increase beyond optimized weight percent, there is effect in the coatings due to the deterioration of the integrity and there is a possibility for agglomeration in nanocomposites at higher concentration. The protection efficiency (*PE*) of the coatings was calculated by using the formula (Equation 1):

$$PE\,(\%) = \frac{I_{corr,bare} - I_{corr,\,coated}}{I_{corr,\,bare}} \times 100. \qquad (1)$$

Where $I_{corr,\,bare}$ and $I_{corr,\,coated}$ are the corrosion current density for uncoated and coated SS 304, respectively.

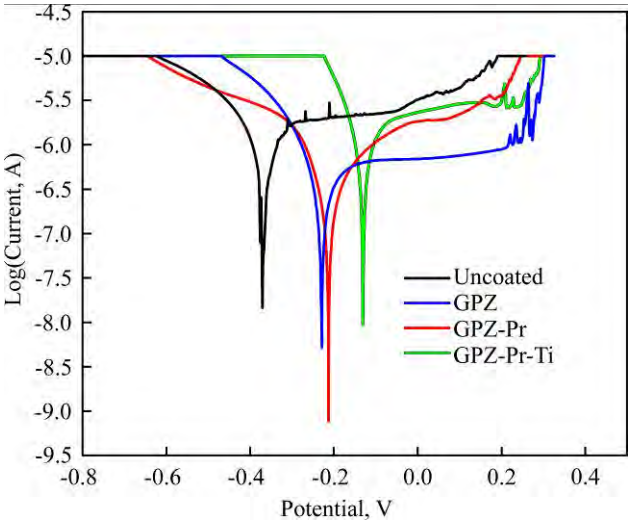

Fig. 9. Potentiodynamic polarization scans for Uncoated, GPZ, GPZ-Pr and GPZ-Pr-Ti.

Table. Electrochemical parameters obtained from the polarization measurements in 0.5M of NaCl solution.

Sample	E_{corr} (mV)	I_{corr} ($\mu A/cm^2$)	Protection	Corrosion rate
Efficiency (%) (mm/y)				
Bare SS 304	-370	5.626	–	0.063
GPZ	-229	4.987	11.35	0.055
GPZ-Pr	-213	2.679	52.38	0.030
GPZ-Pr-Ti	-132	0.126	97.76	1.414×10^{-3}

The polarization curves and the calculated Tafel parameters of the samples after immersion in 0.5M of NaCl solutions are summarized in Table. E_{corr} for bare and GPZ were determined as -370 mV and -229 mV, respectively. E_{corr} is a measure of the tendency of the sample to corrode and the protection efficiency of coatings. As the value of E_{corr} becomes more positive, the efficiency of protection increases. The positive shift in E_{corr} suggests an efficient protection of stainless steel by sol-gel coatings. Also, the measured corrosion for GPZ (i.e., 4.987 $\mu A\cdot cm^{-2}$) is lower than the corrosion current for bare SS 304 (i.e., 5.626 $\mu A\cdot cm^{-2}$). After the addition of Pr_6O_{11}-TiO_2 nanocomposites, there is a positive shift in E_{corr} value as well as a decrease in corrosion current. As shown in Table, the protection efficiency for GPZ-Pr-Ti is calculated as 97.76%, which is much higher than the protection efficiency of GPZ (11.35%). The corrosion rate is known to significantly decrease after the addition of the nanocomposites (Pr_6O_{11}-TiO_2). These results show the effect of preventing water from diffusing through the coating. The surfaces are deprived of oxygen and thus, extend at which the cathodic reaction happens is very limited. The protection efficiency and corrosion rate results reveal that the GPZ-Pr-Ti coated on SS 304 effectively protects the substrate and improves the corrosion resistance due to the homogeneous distribution of nanocomposites and relatively less porous surface of GPZ-Pr-Ti hindered the access of electrolyte to the substrate.

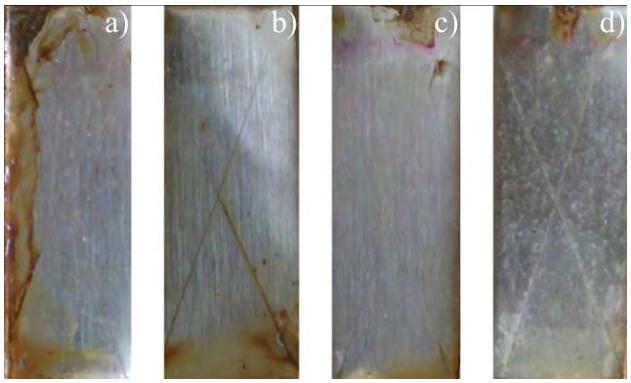

Fig. 10. Corrosion tested substrate after 480h in the salt spray chamber (a) Uncoated SS 304; (b) GPZ; (c) GPZ-Pr and (d) GPZ-Pr-Ti.

Salt spray test

The more traditional salt spray technique was used to investigate the corrosion performance of the SiO_2 @ Pr_6O_{11}-TiO_2 films coated on SS 304. The coated plates were exposed in salt spray chamber for 480h (20 days) are shown in Fig. 10 (taped areas were cropped and specifically corrosion affected portions were taken). It can be clearly seen that GPZ-Pr-Ti exhibits less corrosion and retains their coating without any peel and crack on the surface. The bare SS 304 on contrast exhibits early signs of corrosion. The EIS results are in good agreement with visual observation. Therefore, the data confirm that SiO_2 @ Pr_6O_{11}-TiO_2 coatings have good anti-corrosion behavior facilitating the corrosion inhibition comrade when compare to the other silane coatings.

CONCLUSIONS

This work illustrates the encapsulation of Pr_6O_{11}-TiO_2 by SiO_2 layer to form core-shell microstructures. The superior performance can be attributed to the siloxane coatings combined with Pr_6O_{11}-TiO_2 to protect the substrate anodically. The fabrication process was easily controlled by varying the composition of nanocomposites. The results indicated that the optimal composition of Pr_6O_{11}-TiO_2 (0.5 wt%)/SiO_2 showed an excellent anticorrosion effect for SS 304 in 0.5M NaCl solution. In comparison, GPZ and GPZ-Pr deteriorate the coating integrity by introducing diffusion paths for aggressive electrolyte species, which results in a loss of anti-corrosion efficiency. The best passive and active corrosion resistances were provided by the GPZ-Pr-Ti coating, as determined by EIS analysis. To the best of our knowledge, SiO_2 @ Pr_6O_{11}-TiO_2 hybrid materials have not been reported earlier. It is believed that this offer an effective strategy and promising industrial application for fabricating anticorrosion coatings on other metallic materials.

ACKNOWLEDGEMENTS

The authors are grateful to the Defence Research and Development Organization (DRDO), Government of India, New Delhi for their financial support.

REFERENCES

1. Guin A.K., Nayak S., Rout T.K., Bandyopadhyay N. and Sengupta D.K. Corrosion Resistance Nano-hydrid Sol-Gel Coatings on Steel Sheet. *ISIJ Int.* 2011, **51**(3), 435–440.
2. Celik E., Yildiz A.Y., Ak Azem N.F., Tanoglu M., Toparli M., Emrullahoglu O.F. and Ozdemir I. Preparation and Characterization of Fe_2O_3–TiO_2 thin Films on Glass Substrate for Photocatalytic Applications. *Mater Sci Eng*. 2006, **129**, 193–199.
3. Leng Y.X., Huang N., Yang P., Chen J.Y., Sun H., Wang J., Wan G.J., Leng Y. and Chu P.K. Influence of Oxygen Pressure on the Properties and Biocompatibility of Titanium Oxide Fabricated by Metal Plasma Ion Implantation and Deposition. *Thin Solid Films*. 2002, **420**, 408–413.
4. Khojier K., Savaloni H., Kangarloo H., Ghoranneviss M. and Yari M. Influence of Annealing Temperature on the Nanostructure and Corrosivity of Ti/Stainless Steel Substrates. *Appl Surf Sci*. 2008, **254**, 2528–2533.
5. Sheng Y., Liang L., Xu Y., Wu D. and Sun Y. Low-temperature Deposition of the High-performance Anatase-titania Optical Films via a Modified Sol–gel Route. *Opt Mater*. 2008, **30**, 1310–1315.
6. Yun H., Li J., Chen H. and Lin Ch. A Study on the N-, S- and Cl-modified Nano-TiO_2 Coatings for Corrosion Protection of Stainless Steel. *Electrochim Acta*. 2007, **52**, 6679–6685.
7. Johnson B.Y., Edington J. and O'Keefe M.J. Effect of Coating Parameters on the Microstructure of Cerium Oxide Conversion Coatings. *Mater Sci Eng*. 2003, **A361**, 225–231.
8. Balamurugan A., Kannan S. and Rajeswari S. Evaluation of TiO_2 Coatings Obtained Using the Sol–gel Technique on Surgical Grade Type 316L Stainless Steel in Simulated Body Fluid. *Mater Lett*. 2005, **59**, 3138–3143.
9. Karpagavalli R., Zhou A.H., Chellamuthu P. and Nguyen K. Corrosion Behavior and Biocompatibility of Nanostructured TiO_2 Film on Ti_6Al_4V. *J Biomed Mater Res*. 2007, **83A**, 1087–1095.
10. Permpoon S., Fallet M., Berthome G., Baroux B., Joud J.C. and Langlet M. Photo Induced Hydrophilicity of TiO_2 Films Deposited on Stainless Steel via Sol-gel Technique. *J Sol-Gel Sci Techn*. 2005, **35**, 127–135.
11. Nazeri A., Trzaskoma P.P. and Bauer D. Synthesis and Properties of Cerium and Titanium Oxide thin Coatings for Corrosion Protection of 304 Stainless Steel. *J Sol–Gel Sci Technol*. 1997, **10**, 317–331.
12. Mekeridis E.D., Kartsonakis I.A. and Kordas G.C. Multilayer Organic–inorganic Coating Incorporating TiO_2 Nanocontainers Loaded with Inhibitors for Corrosion Protection of AA2024-T3. *Prog Org Coat.* 2012, **73**, 142–148.
13. Legrand C., Malibert C. and Bach S. Elaboration and Characterization of thin Films of TiO_2 Prepared by Sol–gel Process. *Thin Solid Films*. 2002, **418**, 79–84.
14. Zhai T., Xie S., Lu X., Xiang L., Yu M., Li W., Liang C., Mo C., Zeng F., Luan T. and Tong Y. Porous $Pr(OH)_3$ Nanostructures as High-Efficiency Adsorbents for Dye Removal. *Langmuir*. 2012, **28**, 11078–11085.
15. Moudler J.F., Stickle W.F., Sobol P.E. and Bomben K.D. *Handbook of X-Ray Photoelectron Spectroscopy*. (Ed.: J. Chastain), Perkin-Elmer, Corp: Eden Prairie, 1992. P. 261.
16. Wagner C.D., Riggs W.M., Davis L.E. and Moulder J.F. *Handbook of X-ray Photoelectron Spectroscopy*. Perkin Elmer, Eden Prairie, 1979. pp. 81.
17. He H., Dai H.X., Wong K.W. and Au C.T. $RE_{0.6}Zr_{0.4-x}Y_xO_2$ (RE = Ce, Pr; x = 0, 0.05) Solid Solutions: An Investigation on Defective Structure, Oxygen Mobility, Oxygen Storage Capacity, and Redox Properties. *Appl Catal A-Gen*. 2003, **251**, 61–74.
18. Madhankumar A. and Rajendran N. A Promising Copolymer of *p*-phenylendiamine and *o*-aminophenol: Chemical and Electrochemical Synthesis, Characterization and its Corrosion Protection Aspect on Mild Steel. *Synt Met*. 2012, **162**, 176–185.

Received 18.11.14
Accepted 06.02.15

Реферат

В статье описывается попытка разработки антикоррозионных покрытий для стали SS 304 на основе силоксановых композиционных пленок с Pr_6O_{11}-TiO_2 наночастицами, получаемых золь-гель методом.

Показано, что при использовании нанокомпозитов из оксида празеодима, легированного оксидом титана (Pr_6O_{11}-TiO_2), внедренных в гибридный золь-гель слой, достигается эффективная защита от коррозии нижележащей стальной подложки. Влияние Pr_6O_{11}-TiO_2 дает удивительные аспекты на основе активных антикоррозионных покрытий. Силиказоль обрабатывали Pr_6O_{11}-TiO_2 для достижения содержания 0–1% мас. нанокомпозитов. Влияние различного содержания нанокомпозитов на матрицу из диоксида кремния для повышения антикоррозионной стойкости исследовали с помощью электрохимической импедансной спектроскопии (ЭИС). Нанокомпозиты Pr_6O_{11}-TiO_2, внедренные в гибридной золь-гель слой, эффективно защищают подложку от коррозии. Результаты показали значительное улучшение антикоррозийных свойств с ростом содержания добавок вплоть до оптимизированной концентрации нанокомпозитов. Для характеризации морфологии поверхности легированных и нелегированных покрытий применяли просвечивающую электронную микроскопию (ПЭМ) и сканирующую электронную микроскопию (СЭМ). Исследования показали, что наличие синергетического эффекта между Pr_6O_{11}-TiO_2 и силоксановой матрицей приводит к самовосстановлению покрытий.

Ключевые слова: золь-гель процесс, антикоррозия, нанокомпозиты, электрохимическая импедансная спектроскопия.